

Antenna Showers with Hadronic Initial States

M. Ritzmann^a, D. A. Kosower^a, P. Skands^b

^a*Institut de Physique Théorique, CEA Saclay, F-91191 Gif-sur-Yvette cedex, France*

^b*CERN TH, Geneva 23, CH-1211, Switzerland*

Abstract

We present an antenna shower formalism including contributions from initial-state partons and corresponding backwards evolution. We give a set of phase-space maps and antenna functions for massless partons which define a complete shower formalism suitable for computing observables with hadronic initial states. We focus on the initial-state components: initial–initial and initial–final antenna configurations. The formalism includes comprehensive possibilities for uncertainty estimates. We report on some preliminary results obtained with an implementation in the `VINCIA` antenna-shower framework.

Keywords: parton showers; quantum chromodynamics; hadronic collisions

1. Introduction

Parton-shower algorithms offer a universal and fully exclusive perturbative resummation framework for high-energy processes. In the context of Monte Carlo event generators [1], they also provide the perturbative input for hadronization models. As such, they are complementary to more inclusive techniques, such as fixed-order calculations (limited to small numbers of hard and well-separated partons) and more inclusive resummation approaches (limited to a fixed set of observables).

Sjöstrand derived the first consistent parton-shower algorithm [2] for so-called “backwards evolution” of initial-state partons a quarter-century ago. The central point is that an initial-state parton defined at a high factorization scale, Q_F , can be evolved “backwards”, towards earlier times, to find the parton from which it originated at some low scale, $Q_0 \sim 1$ GeV. During this evolution, which is governed by the Altarelli-Parisi splitting kernels [3] supplemented by PDF ratios (a point which is crucial to the backwards-evolution formalism), initial-state radiation is emitted, which in turn gives rise to its own final-state radiation, and

the character of the evolving parton changes, migrating towards successively higher x values and towards the more valence-dominated flavor content at low Q .

As an alternative to Altarelli-Parisi evolution, Gustafson and Pettersson proposed a final-state algorithm based on QCD dipoles [4], which has been implemented in `ARIADNE` [5]. There, however, initial-state radiation does not rely on backwards evolution. Instead, it is treated essentially as final-state radiation off dipoles stretched between the hard process and the beam remnants, and thus depends on the non-perturbative makeup of the remnants. Winter and Krauss took a first step towards combining the dipole formalism with backwards evolution (and thus also eliminating the dependence on the remnants) in ref. [6]. Our construction differs in the antenna functions, evolution variables, and recoil strategy. In particular, it differs in the treatment of collinear singularities in initial–final antennæ. We have checked that our antennæ properly reproduce all QCD singularities.

A complementary approach which merges the Lund dipole language with that of fixed-order antenna factorization [7, 8, 9, 10], is that of `VINCIA`

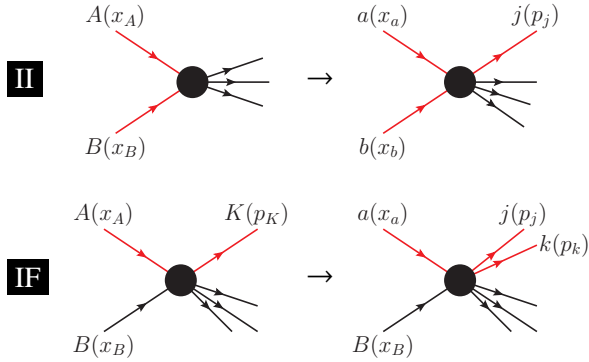


Figure 1: Illustration of initial–initial and initial–final branchings: $AB \rightarrow ajb$ and $AK \rightarrow ajk$, respectively. For the II case, the recoil of the hard system is illustrated by the change in orientation of the three outgoing lines representing the original final-state system.

cia [11, 12, 13]. (Note: we henceforth use the term “antenna” rather than “dipole” to avoid ambiguities of historical origins, see e.g., ref. [14]). So far, however, the VINCIA formalism has been applied only to final-state showers. In this paper, we present all the ingredients necessary to construct a consistent initial-state shower based on QCD antennæ. A further important ingredient is comprehensive possibilities for uncertainty estimates, in line with the framework for automated theory uncertainties proposed in ref. [15].

2. Antennæ and Antenna Showers

Throughout this Letter, we use the following notation convention: capital letters for pre-branching (parent) partons and lower-case letters for post-branching (daughter) ones. Also, we use the first letters of the alphabet, a, b, c, \dots , for incoming partons and letters starting from i, j, k, \dots for outgoing ones. Fig. 1 illustrates these choices for the two basic types of configurations we consider. We will also mark incoming particles with a minus sign in front in antenna functions. We adopt the convention that particle energies are always positive, whether the particle is in the initial or the final state. As a result, $s_{ij} = (k_i + k_j)^2$ is always positive.

The key building block for parton showers is the Sudakov factor, which represents the non-emission

probability between two values of the evolution scale, see [1, 16] for reviews. In the context of an antenna shower, the Sudakov factor for the branching of one antenna is

$$\Delta(Q_{\text{start}}^2, Q_{\text{emit}}^2) = \exp[-\mathcal{A}(Q_{\text{start}}^2, Q_{\text{emit}}^2)], \quad (1)$$

with

$$\mathcal{A}(Q_{\text{start}}^2, Q_{\text{emit}}^2) = \int_{Q_{\text{start}}^2}^{Q_{\text{emit}}^2} a_c \frac{f_a(x_a, Q^2)}{f_A(x_A, Q^2)} \frac{f_b(x_b, Q^2)}{f_B(x_B, Q^2)} d\Phi_{\text{ant}}. \quad (2)$$

In this equation, $d\Phi_{\text{ant}}$ represents the antenna phase-space factorization, which provides an exact Lorentz-invariant mapping from 2 to 3 on-shell partons, that conserves global energy and momentum. Specific forms appropriate to initial–final and initial–initial antenna configurations are defined in sections 3 and 4, respectively.

The evolution variable Q^2 is a function of the phase-space point and must vanish in the unresolved limits [17]. The general formalism permits us to study different evolution variables [11, 15], though in this Letter we will restrict ourselves to a transverse-momentum type variable, defined in section 5. As in all parton showers, the description is expected to be accurate only in the strongly-ordered limit for the Q^2 of successive emissions.

The dressed or colored antenna function a_c is defined as¹

$$a_c = 4\pi\alpha_S(Q^2)C\bar{a}, \quad (3)$$

where C is a color factor (we recall that we use normalization conventions such that gluon and quark emission antennæ have $C = C_A$ and $C = 2C_F$, respectively, and gluon-splitting ones have $C = 1$), and \bar{a} is a color-ordered antenna function, which embodies the factorization of QCD matrix elements in all single-unresolved soft and collinear limits. We don’t take the functions \bar{a} to be fixed; instead we use different antenna functions with the same singular limits as one estimate of the shower uncertainty.

¹ Note that in [15] the normalization was $a_c = \alpha_S/(4\pi)C\bar{a}$

We use so-called global antenna functions [4] (called sub-antenna functions with uniquely identified radiators in ref. [9]) which are active over all of phase space. A backwards-evolution shower based on sector antennæ in analogy to refs. [18, 13] is left for future work. Some, but not all, antennæ needed for initial-state radiation can be chosen to be the crossings of their final-final counterparts. An incoming particle is necessarily a hard radiator in an antenna. Therefore, a gluon emission antenna function with an incoming gluon has to reproduce the AP splitting function on its own, e. g.

$$\bar{a}(-a_g, j_g, k_x) \xrightarrow{p_j \rightarrow z p_a} \frac{1}{s_{aj}} \frac{1}{1-z} P_{gg \rightarrow G}(1-z) \quad (4)$$

whereas if both gluons are in the final state, the collinear singularity is reproduced by the sum of two antenna functions

$$\bar{a}(h_x, i_g, j_g) + \bar{a}(i_g, j_g, k_x) \xrightarrow{p_j \rightarrow z p_i} \frac{1}{s_{ij}} P_{gg \rightarrow G}(z) \quad (5)$$

where the first antenna function is singular for i becoming soft, the second for j .

In pure final-state showers, the x values of the incoming partons are not modified by the phase-space factorization, hence the PDF ratios in eq. (2) drop out, yielding the ordinary form of the final-final Sudakov form factor [11, 15].

For initial-final antennæ, only one of the PDF x values changes, and a Sudakov factor very similar to that of conventional AP showers results, with a single PDF ratio in the kernel, $f_a(x_a, Q^2)/f_A(x_A, Q^2)$. Unlike conventional showers, however, we must also consider the backwards evolution of two initial-state partons simultaneously, generally requiring two separate parton-density factors in initial-initial antennæ.

The consideration of initial-initial and initial-final antennæ gives rise to one more subtlety. The basic antenna functions are color-ordered, so that in a final-final gluon-emission antenna, for example, the emitted gluon is color adjacent to both other (hard) daughter partons. That is, it is the middle parton of the color trio which is emitted. The leading-color approximation inherent in parton showers along with the symmetry of final-state

phase space allows us only antennæ with this ordering. When considering initial-state antennæ, however, the emitted parton need not be color-adjacent to both other daughter partons; the middle parton, adjacent to both, may end up in the initial instead of the final state. We will call antennæ in which the middle parton is emitted into the final state, ‘emission’ antennæ; and those in which the middle parton ends up in the initial state, ‘conversion’ antennæ.

For those antennæ in which the type (spin) of the initial-state partons does not change after branching, we can redistribute collinear singularities to neighboring antennæ so as to replace ‘conversion’ antennæ by ‘emission’ antennæ. For those antennæ in which the type of the initial-state partons changes during branching — in which a quark backwards-evolves into a gluon or vice versa — we cannot avoid a consideration of both types of antenna function and non-emission probability.

3. Initial-Final Configurations

The pre- and post-branching partons for initial-final configurations are labeled by $AK \rightarrow ajk$, with the other incoming parton, B , acting as a passive spectator, see the illustration in fig. 1.

In general, the incoming momentum after branching will no longer be parallel to the beam direction. We could boost it back to the beam direction; this will transfer some of the transverse momentum generated in the emission to the rest of the event. This is the antenna analog of the recoil considered in ref. [19]. In the present Letter, we will instead restrict the branching so that the incoming momentum remains parallel to the beam axis after branching.

With this restriction, the phase-space factorization reads [20],

$$\int \frac{dx_a}{x_a} d\Phi_3(-a, -c; j, k, R) = \int \frac{dx_A}{x_A} d\Phi_2(-A, -c; K, R) d\Phi_{\text{ant}}^{if}(-A; K \rightarrow -a; j, k) \quad (6)$$

with $x_A/x_a = s_{AK}/(s_{AK} + s_{jk})$ and where the initial-final antenna phase space is

$$d\Phi_{\text{ant}}^{jf}(-A; K \rightarrow -a; j, k) = \frac{1}{16\pi^2} \frac{s_{AK}}{(s_{AK} + s_{jk})^2} ds_{jk} ds_{aj} \quad (7)$$

with the boundaries $0 \leq s_{jk} \leq s_{AK}(1 - x_A)/x_A$, $0 \leq s_{aj} \leq s_{AK} + s_{jk}$. We have suppressed the integration over the third coordinate of the initial-final phase space on which the emission probability does not depend.

The gluon-emission antennæ can be chosen as

$$\bar{a}(-a_q, j_g, k_q) = \frac{1}{s_{AK}} \left(\frac{2s_{ak}s_{AK}}{s_{aj}s_{jk}} + \frac{s_{jk}}{s_{aj}} + \frac{s_{aj}}{s_{jk}} \right) \quad (8)$$

$$\bar{a}(-a_q, j_g, k_g) = \frac{1}{s_{AK}} \left(\frac{2s_{ak}s_{AK}}{s_{aj}s_{jk}} + \frac{s_{jk}}{s_{aj}} + \frac{s_{aj}}{s_{jk}} \frac{s_{ak}}{s_{AK}} \right) \quad (9)$$

$$\bar{a}(-a_g, j_g, k_g) = \frac{1}{s_{AK}} \left(\frac{2s_{ak}s_{AK}}{s_{aj}s_{jk}} + \frac{2s_{jk}s_{AK}}{s_{aj}(s_{ak} + s_{aj})} + \frac{2s_{jk}}{s_{aj}} \frac{s_{ak}}{s_{AK}} + \frac{s_{aj}}{s_{jk}} \frac{s_{ak}}{s_{AK}} \right) \quad (10)$$

$$\bar{a}(-a_g, j_g, b_q) = \frac{1}{s_{AK}} \left(\frac{2s_{ak}s_{AK}}{s_{aj}s_{jk}} + \frac{2s_{jk}s_{AK}}{s_{aj}(s_{ak} + s_{aj})} + \frac{2s_{jk}}{s_{aj}} \frac{s_{ak}}{s_{AK}} + \frac{s_{aj}}{s_{jk}} \right) \quad (11)$$

where it is apparent that the antennæ with an incoming quark are crossings of their final-state counterparts whereas the ones with incoming gluons have additional terms compared to their final-state counterparts to ensure the collinear singularity $a \parallel j$ is taken into account properly.

The antenna for the splitting of a final-state gluon into a quark-antiquark pair is chosen as

$$\bar{a}(-a_x, j_q, k_{\bar{q}}) = \frac{1}{2} \frac{1}{s_{jk}} \frac{s_{aj}^2 + s_{ak}^2}{s_{AK}^2} \quad (12)$$

where the factor 1/2 originates from the fact that the gluon is part of two antennæ.

The antenna governing the backwards-evolution of a gluon into a quark is

$$\bar{a}(-a_q, j_q, k_x) = \frac{1}{2} \frac{1}{s_{aj}} \frac{s_{ak}^2 + s_{jk}^2}{s_{AK}^2} \quad (13)$$

For the reverse process of a sea quark backwards-evolving into a gluon, we use

$$\bar{a}_{\text{conv}}(j_q, -a_g, k_x) = \frac{1}{s_{AK}} \left(\frac{-2s_{jk}(s_{AK} - s_{aj})}{s_{aj}(s_{aj} + s_{ak})} + \frac{s_{ak}}{s_{aj}} \right) \quad (14)$$

with a color connection $j - a - k$ at variance with the other antennæ.

4. Initial-Initial Configurations

For initial-initial antennæ, we label the pre- and post-branching partons by $AB \rightarrow ajb$, see fig. 1. In the initial-initial case, we must necessarily have transverse momentum generated, which must be absorbed by the rest of the event. There are two ways of proceeding. One can allow the incoming partons to be shifted away from the beam direction after branching, and then boost back to a frame in which they are again parallel to the beam direction. Alternatively, one can fix the incoming partons to be parallel to the beam direction, and balance the new transverse momentum by boosting the rest of the event appropriately. In both cases, there is a freedom in how the longitudinal part of the emission momentum is absorbed into the initial state. This corresponds to a freedom in relating the post-branching momentum fractions $x_{a,b}$ to the pre-branching momentum fractions $x_{A,B}$. In the first case, this freedom is parametrized by the recoil or reconstruction function r in combination with the Lorentz transformation boosting back to the lab frame. In the second case, it is parametrized by the functional form of $x_{a,b}$.

It turns out that these two approaches are equivalent, unlike the initial-final case. We define our recoil strategy in terms of $x_{a,b}$ here. The phase-space

factorization reads [21],

$$\begin{aligned} & \int \frac{dx_a}{x_a} \frac{dx_b}{x_b} d\Phi_2(-a, -b; j, R) \\ &= \int \frac{dx_A}{x_A} \frac{dx_B}{x_B} d\Phi_1(-A', -B'; R') d\Phi_{\text{ant}}^{ii} \end{aligned} \quad (15)$$

with the initial–initial antenna phase space

$$\begin{aligned} d\Phi_{\text{ant}}^{ii}(-A', -B' \rightarrow -a, -b; j) = \\ \frac{1}{16\pi^2} \frac{s_{AB}}{s_{ab}^2} \theta(1-x_a) \theta(1-x_b) ds_{aj} ds_{jb} \end{aligned} \quad (16)$$

where we have suppressed the integration over the angle ϕ parametrizing rotations around the beam. The pre- and post-branching momenta are related by a Lorentz transform:

$$\begin{aligned} \Lambda_{\nu}^{\mu}(p_R, p'_R) &= g_{\nu}^{\mu} + \frac{2}{m_R^2} (p'_R)^{\mu} (p_R)_{\nu} \\ &- \frac{2}{(p_R + p'_R)^2} (p_R + p'_R)^{\mu} (p_R + p'_R)_{\nu}. \end{aligned} \quad (17)$$

The phase space boundary depends directly on the definition of the post-branching momentum fractions, which is not fixed completely by the requirements of $x_a x_b s_{AB} = x_A x_B s_{ab}$ and the behavior in the soft and collinear limits.

For gluon emission, we use

$$\frac{x_A}{x_a} = \left(\frac{s_{ab} - s_{jb} s_{AB}}{s_{ab} - s_{aj} s_{ab}} \right)^{1/2}, \quad (18)$$

whereas for conversion, we keep one incoming momentum fixed, i.e. $x_A/x_a = s_{AB}/s_{ab}$, $x_b = x_B$, giving the phase space boundaries $s_{aj} + s_{jb} \leq s_{AB}(1 - x_A)/x_A$. This corresponds to the use of a one-sided factorization, which is possible because only one collinear limit is singular, whereas the behavior of the phase space factorization in the other collinear limit is not constrained.

We use the emission antennæ

$$\bar{a}(-a_q, j_g, -b_q) = \frac{1}{s_{AB}} \left(\frac{2s_{ab}s_{AB}}{s_{aj}s_{jb}} + \frac{s_{aj}}{s_{jb}} + \frac{s_{jb}}{s_{aj}} \right) \quad (19)$$

$$\begin{aligned} \bar{a}(-a_q, j_g, -b_g) &= \frac{1}{s_{AB}} \left(\frac{2s_{ab}s_{AB}}{s_{aj}s_{jb}} + \frac{2s_{aj}s_{AB}}{s_{jb}(s_{ab} + s_{jb})} \right. \\ &\quad \left. + \frac{2s_{aj}s_{ab}}{s_{jb}s_{AB}} + \frac{s_{jb}}{s_{aj}} \right) \end{aligned} \quad (20)$$

$$\begin{aligned} \bar{a}(-a_g, j_g, -b_g) &= \frac{1}{s_{AB}} \left(\frac{2s_{ab}s_{AB}}{s_{aj}s_{jb}} + \frac{2s_{aj}s_{AB}}{s_{jb}(s_{ab} + s_{jb})} \right. \\ &\quad \left. + \frac{2s_{jb}s_{AB}}{s_{aj}(s_{ab} + s_{aj})} + \frac{2s_{aj}s_{ab}}{s_{jb}s_{AB}} + \frac{2s_{jb}s_{ab}}{s_{aj}s_{AB}} \right) \end{aligned} \quad (21)$$

For a quark backwards-evolving into a gluon, we use

$$\bar{a}(j_q, -a_g, -b_x) = \frac{1}{s_{AB}} \left(-\frac{2s_{jb}s_{AB}}{s_{aj}(s_{ab} - s_{aj})} + \frac{s_{ab}}{s_{aj}} \right) \quad (22)$$

The antenna for a gluon backwards-evolving into a quark is the crossing of the initial–final counterpart:

$$\bar{a}(-a_x, j_q, -b_q) = \frac{1}{2} \frac{1}{s_{jb}} \frac{s_{aj}^2 + s_{ab}^2}{s_{AB}^2} \quad (23)$$

5. Implementation and Preliminary Results

In the antenna shower, as in a conventional shower, we start the evolution at high Q^2 , and generate a series of branchings at successively lower Q^2 , stopping when we reach a shower cut-off, typically around 1 GeV. Each branching is generated according to the non-emission probability (1), and in this Letter we shall restrict ourselves to strict strong ordering, postponing a discussion of smooth ordering [15] and/or power showers [22] to a subsequent study.

In order to generate a branching, we must invert the function specified by the integral (2). This is in general a difficult task even if the integral is doable analytically, because the result involves dilogarithms. In some cases, the boundaries even make it unreasonable to perform the integral analytically. A direct inversion would in either case be quite slow. Instead, we proceed as follows. We pick a simple function — a trial antenna function a_c^{trial} and trial ratios of parton-density functions $R_{\text{pdf}}^{\text{trial}}$ — which *overestimates* the integrand,

and veto the excess emissions generated according to the non-emission probability computed using the trial function. The trial function is chosen to capture the leading logarithmic singularities of the antenna function, and to allow the phase-space integral to be factorized into a product of one-dimensional integrals. Where possible, it is also chosen to produce an analytically invertible integral. In the final–final case, the latter requirement can always be satisfied; in initial–initial and initial–final cases, it can be satisfied for most trial antennæ. In the exceptional cases, we employ a two-stage veto. In these cases, the first-level trial function still serves to simplify the inversion of the non-emission probability by ensuring the factorization of the integral into a product of one-dimensional integrals. The veto probability is given by,

$$P_{\text{accept}} = \frac{a_c}{a_c^{\text{trial}}} \frac{R_{\text{pdf}}}{R_{\text{pdf}}^{\text{trial}}}, \quad (24)$$

evaluated at the post-branching kinematic point. In this equation,

$$R_{\text{pdf}} = \frac{f_a(x_a, Q^2) f_b(x_b, Q^2)}{f_A(x_A, Q^2) f_B(x_B, Q^2)} \quad (25)$$

is the ratio of parton densities that appears in eq. (2).

When approaching a heavy flavor threshold, R_{pdf} diverges. As is standard in backwards-evolution codes, we absorb the leading divergent behavior of R_{pdf} into the trial integration to maintain a reasonable efficiency [23]. Analogous issues may arise at large x and low Q^2 in light-quark parton densities due to numerical instabilities. We defer their treatment to future work.

To define a concrete shower algorithm based on the above antennæ and phase-space factorizations, we have chosen to use two different evolution variables, depending on the type of antenna. For gluon emission, we use a transverse momentum,

$$Q_{\perp}^2 = \frac{2s_{ij}s_{jk}}{s_{ij} + s_{jk} + s_{ik}}. \quad (26)$$

For final-state branchings, Q_{\perp}^2 is equal to $2p_{\perp A}^2$, the evolution measure used in ARIADNE [5] (note: pre-

vious VINCIA publications used $4p_{\perp A}^2$). The maximal value of Q_{\perp}^2 in the final-state case is $s_{ijk}/2$. For conversion and gluon splitting antennæ, we instead use the virtuality of the only potentially singular propagator as the evolution variable. As in the final-state shower [11, 12, 15], other choices are possible within the VINCIA formalism. We defer an exploration of more general possibilities to future work.

We now turn to a few basic tests of each component of the shower algorithm. In all cases, we consider pp collisions at 8 TeV CM energy, use the MSTW 2008 LO PDF set [24], with a one-loop running α_S , normalized to $\alpha_S(m_Z) = 0.13939$. In all calculations performed here, we turn off hadronization and primordial k_T , as well as the underlying event, both in the VINCIA calculation and in the PYTHIA 8 [25] calculations to which we compare. While the evolution variables in VINCIA and PYTHIA are different, we have tried to match the shower cut-offs in calculations with the latter to that we use in VINCIA. This includes accounting for the difference in normalization between limiting definitions of transverse momentum. Note that while VINCIA uses a zero-mass variable flavor number scheme, PYTHIA 8 uses the physical quark masses everywhere. For the observables we discuss here, the effect is negligible.

In fig. 2, we show the p_T spectrum of the Z boson in Drell-Yan production, which is sensitive to radiation in initial–initial configurations. The main figure pane shows the peak of the distribution, while the inset shows the high- p_T tail. The figure shows VINCIA curves computed using two different antenna functions: the default antenna given earlier, and an enhanced antenna function, with a finite term $— 5/s_{ijk} —$ added. It also shows the result obtained with PYTHIA 8.

The overall shape of the three curves is similar: small values at small p_T , rising to a peak and then declining again with a rough power-law fall in the asymptotic region, and a “knee” around $p_T \sim 90$ GeV due to the requirement of strong ordering which we have imposed here. The difference between the two VINCIA predictions illustrates the un-

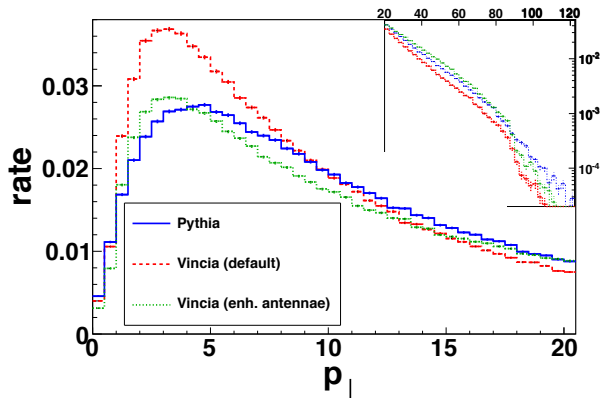


Figure 2: The Drell-Yan p_T spectrum. The dashed red curve shows the value computed using VINCIA with default antennae functions, while the dotted green curve shows the VINCIA predicted with an enhanced antenna function. The solid blue curve gives the PYTHIA 8 prediction. The inset shows the high- p_T tail.

certainty due to the shower function and in particular higher-order terms in the shower. The difference shown here is illustrative only; a more extensive exploration of possible antenna variations would be required before taking the spread as a quantitative estimate of the uncertainty. We may nonetheless observe that the PYTHIA 8 reference calculation differs from the VINCIA one (with default antenna) by roughly the same amount in the peak region as does the enhanced VINCIA prediction. This illustrates a tradeoff between a more active recoil strategy (PYTHIA) and a more active radiation pattern (enhanced VINCIA), which will be interesting to study more closely. At large p_T , all three curves are close to each other; the transverse momentum here is dominated by the recoil against hard lone-gluon emission. This region would be described well by fixed-order calculations.

For initial-final configurations, coherence is particularly important, and can lead to sizable asymmetries (see, e.g., [26]). An illustration of the effect is given in fig. 3, which shows $qq \rightarrow qq$ scattering with two different color-flow assignments: forward (left) and backward (right). In both cases, the starting scale of the shower evolution would be \hat{p}_T , the transverse-momentum scale characterizing the hard scattering. Coherence, however, im-

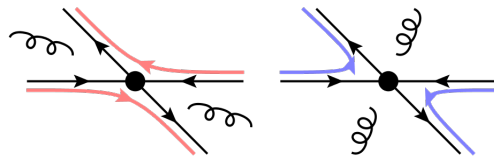


Figure 3: Different color flows and corresponding emission patterns in $qq \rightarrow qq$ scattering. The straight (black) lines are quarks with arrows denoting the direction of motion in the initial or final states, and the curved (colored) lines indicating the color flow. The beam axis is horizontal, and the vertical axis is transverse to the beam. The initial-state momenta would be reversed in a Feynman diagram, so that the gluon emissions symbolically indicated by curly lines would be inside the corresponding color antennae. Forward flow is shown on the left, and backward flow on the right.

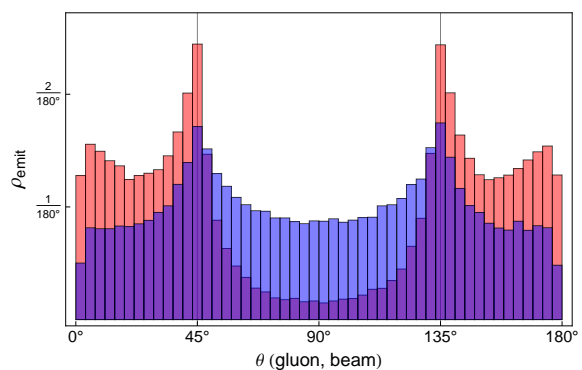


Figure 4: Angular distribution of the first gluon emission in $qq \rightarrow qq$ scattering at 45° , for the two different color flows. The light (red) histogram shows the emission density for the forward flow, and the dark (blue) histogram shows the emission density for the backward flow.

plies that radiation should be directed primarily inside the color antenna, so that in the forward flow it would be directed towards large rapidity, and strongly suppressed at right angles to the beam direction. In the backward flow, conversely, radiation at right angles to the beam should be unsuppressed. The two radiation patterns are illustrated schematically by the gluons in fig. 3. The intrinsic coherence of the antenna formalism accounts for this effect automatically. That VINCIA reproduces this feature is demonstrated in fig. 4, which shows the angular distribution of the first emitted gluon for the forward and backward color flows, respectively, for a scattering angle of 45° and $\hat{p}_T = 100$ GeV. The distributions clearly show that the backward color

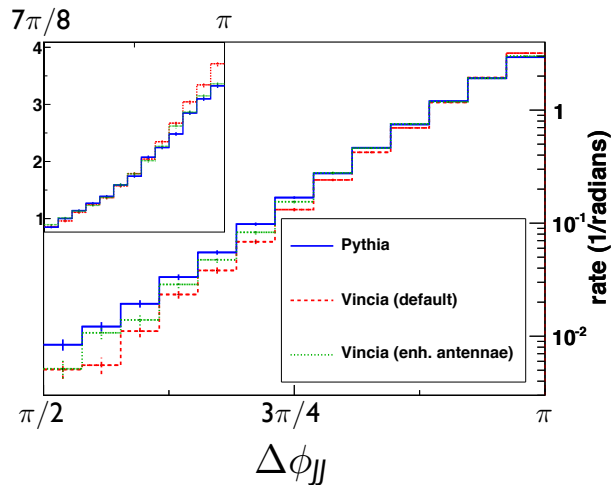


Figure 5: The dijet decorrelation angle. The histograms are normalized to unity separately.

flow allows for much more radiation at 90° than the forward one. The p_T spectrum of the radiation (not shown) is also harder. The next step will be to interface the hadronization and underlying-event models in PYTHIA, and compare to experimental studies, such as the one by CDF [27] (we note that an update of that study, correcting it to the hadron level, would be highly useful to the MC community).

Finally, to demonstrate the combination of all shower components acting together, we show the dijet decorrelation angle (the azimuthal angle between the two leading jets), $\Delta\phi_{JJ}$, in fig. 5. Using FASTJET [28], we consider anti- k_T jets with radius parameter $R = 0.4$. We demand the two leading jets to have transverse momentum above 100 GeV and to be at rapidities $|y| < 2.8$. Note that PYTHIA 8 produces about 40% more jet events which pass these cuts than VINCIA both with or without enhanced antenna functions, partly due to its more active recoil strategy, which allows the original dijet system to build up transverse momentum successively during the shower cascade. This difference is not visible in fig. 5, as the distributions are all normalized to unity. The two VINCIA distributions are broadly similar to the PYTHIA 8 distribution, and very similar in the two-jet region ($\Delta\phi_{JJ} \sim \pi$) where the parton-shower approximation should be reliable. The differences are substantial in the region below

$\Delta\phi_{JJ} < 3\pi/4$, where hard real emission is important. In this region, fixed-order calculations should be reliable, but unmatched parton showers will not be. Nonetheless, the difference between the VINCIA calculation with default antenna strength and the PYTHIA 8 calculation is similar to that between the two VINCIA calculations, suggesting again that the variation provides a good qualitative assessment of the uncertainty. We defer a comparison of this distribution with fixed-order calculations to future studies.

6. Conclusion and Outlook

In this Letter, we have presented the outline of a formalism for an antenna shower for hadron collisions, along with results from an initial implementation as a plug-in to PYTHIA 8. The formalism requires the introduction of new antennae, corresponding to one or both parents being initial-state partons. These should be further subdivided into the new categories of emission and conversion antennae based on their color flows. The formalism also requires factorizations suitable for phase spaces involving initial-state partons, and introduces ratios of parton densities into the non-emission probabilities governing the shower evolution.

We have chosen to implement the shower as a plug-in to the PYTHIA 8 program, which takes advantage of the latter's flexible framework and makes use of its utilities, structures, and overall management of the branching process. In this approach, it replaces PYTHIA's shower with an antenna shower. For practical and efficiency reasons, we uniformly adopt a trial-and-veto algorithm for generating branchings. The trial functions used in the implementation will be described elsewhere.

We expect to implement further optimizations of the branching step in future work. The leading-order matching approach described in ref. [15] should carry over to the initial-state showering described here, and will be an important next step for the development of VINCIA.

Acknowledgments

The work of MR and DAK was supported by the European Research Council under Advanced Investigator Grant ERC–AdG–228301.

References

- [1] A. Buckley, J. Butterworth, S. Gieseke, D. Grellscheid, S. Höche, et al., General-purpose event generators for LHC physics, *Phys.Rept.* 504 (2011) 145.
- [2] T. Sjöstrand, A Model for Initial State Parton Showers, *Phys.Lett.* B157 (1985) 321.
- [3] G. Altarelli, G. Parisi, Asymptotic Freedom in Parton Language, *Nucl.Phys.* B126 (1977) 298.
- [4] G. Gustafson, U. Pettersson, Dipole Formulation of QCD Cascades, *Nucl.Phys.* B306 (1988) 746.
- [5] L. Lönnblad, ARIADNE version 4: A Program for simulation of QCD cascades implementing the color dipole model, *Comput.Phys.Commun.* 71 (1992) 15.
- [6] J.-C. Winter, F. Krauss, Initial-state showering based on colour dipoles connected to incoming parton lines, *JHEP* 0807 (2008) 040.
- [7] D. A. Kosower, Antenna factorization of gauge theory amplitudes, *Phys.Rev.* D57 (1998) 5410.
- [8] D. A. Kosower, Antenna factorization in strongly ordered limits, *Phys.Rev.* D71 (2005) 045016.
- [9] A. Gehrmann-De Ridder, T. Gehrmann, E. N. Glover, Antenna subtraction at NNLO, *JHEP* 0509 (2005) 056.
- [10] A. Daleo, T. Gehrmann, D. Maitre, Antenna subtraction with hadronic initial states, *JHEP* 0704 (2007) 016.
- [11] W. T. Giele, D. A. Kosower, P. Z. Skands, A Simple shower and matching algorithm, *Phys.Rev.* D78 (2008) 014026.
- [12] A. Gehrmann-De Ridder, M. Ritzmann, P. Skands, Timelike Dipole-Antenna Showers with Massive Fermions, *Phys.Rev.* D85 (2012) 014013.
- [13] J. Lopez-Villarejo, P. Skands, Efficient Matrix-Element Matching with Sector Showers, *JHEP* 1111 (2011) 150.
- [14] Z. Bern, et al., The NLO multileg working group: Summary report (2008). [ArXiv:0803.0494](https://arxiv.org/abs/0803.0494).
- [15] W. Giele, D. Kosower, P. Skands, Higher-Order Corrections to Timelike Jets, *Phys.Rev.* D84 (2011) 054003.
- [16] J. Beringer, et al., Review of Particle Physics (RPP), *Phys.Rev.* D86 (2012) 010001.
- [17] P. Z. Skands, S. Weinzierl, Some remarks on dipole showers and the DGLAP equation, *Phys.Rev.* D79 (2009) 074021.
- [18] A. J. Larkoski, M. E. Peskin, Spin-Dependent Antenna Splitting Functions, *Phys.Rev.* D81 (2010) 054010.
- [19] S. Plätzer, S. Gieseke, Coherent Parton Showers with Local Recoils, *JHEP* 1101 (2011) 024.
- [20] S. Catani, M. Seymour, A General algorithm for calculating jet cross-sections in NLO QCD, *Nucl.Phys.* B485 (1997) 291–419.
- [21] S. Catani, M. Seymour, The Dipole formalism for the calculation of QCD jet cross-sections at next-to-leading order, *Phys.Lett.* B378 (1996) 287–301.
- [22] T. Plehn, D. Rainwater, P. Z. Skands, Squark and gluino production with jets, *Phys.Lett.* B645 (2007) 217–221.
- [23] T. Sjöstrand, P. Z. Skands, Transverse-momentum-ordered showers and interleaved multiple interactions, *Eur.Phys.J.* C39 (2005) 129–154.
- [24] A. Martin, W. Stirling, R. Thorne, G. Watt, Parton distributions for the LHC, *Eur.Phys.J.* C63 (2009) 189–285.
- [25] T. Sjöstrand, S. Mrenna, P. Z. Skands, A Brief Introduction to PYTHIA 8.1, *Comput.Phys.Commun.* 178 (2008) 852.
- [26] P. Skands, B. Webber, J. Winter, QCD Coherence and the Top Quark Asymmetry, *JHEP* 1207 (2012) 151.
- [27] F. Abe, et al., Evidence for color coherence in $p\bar{p}$ collisions at $\sqrt{s} = 1.8$ TeV, *Phys.Rev.* D50 (1994) 5562–5579.
- [28] M. Cacciari, G. P. Salam, G. Soyez, FastJet User Manual, *Eur.Phys.J.* C72 (2012) 1896.